ACS APPLIED NANO MATERIALS

Open Access

This article is licensed under CC-BY 4.0

www.acsanm.org

Article

ZnO Nanorod-Immobilized Polyurethane Foams for Efficient Removal of Gaseous Volatile Organic Compounds

Memnune Kardeş,* Bekir Dizman,‖ Koray Öztürk,‖ and Derya Y. Köseoğlu-İmer‖

Cite This: *ACS Appl. Nano Mater.* 2025, 8, 7290−7303

Read Online

ACCESS | Metrics & More | Article Recommendations | Supporting Information

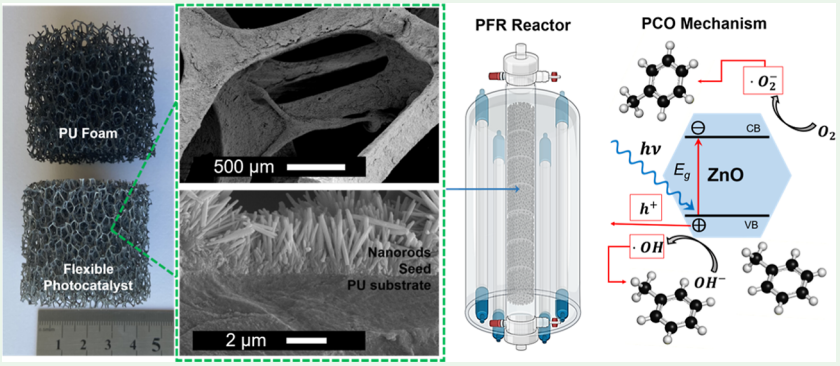

ABSTRACT: Nanoscale semiconductor materials are highly effective catalysts due to their high surface-to-volume ratio, enhanced charge carrier separation, and increased active site density. Integrating them into three-dimensional porous supports optimizes mass transport, facilitating efficient adsorption of volatile organic compounds (VOCs) and catalytic interactions. A flexible hybrid photocatalyst was designed by immobilizing zinc oxide (ZnO) nanorods (NR) on the three-dimensional polyurethane (PU) foam support. The polymer surface was functionalized by chemical solution treatment to increase the adhesion between the catalyst and the surface. ZnO NRs were grown on all strut surfaces of the PU foam via a seed-mediated approach. Photocatalytic experiments were carried out in a laboratory-scale plug flow type photoreactor under UVA light irradiation. The effects of parameters such as initial concentration (ppm), relative humidity (RH) (from 0% to 65%), air flow rate (0.3, 0.6, and 1 L/min), and temperature (from 21 to 35 °C) on the gas phase toluene, ethylbenzene, and chlorobenzene removal were evaluated. In the presence of RH, photoreactions accelerated, leading to an increase in the CO_2 conversion rate. The optimum RH value was determined as 30% according to the maximum removal rate. Similarly, removal efficiencies were improved at temperatures higher than room temperature, and the optimum temperature was evaluated as 30 °C. However, as the initial concentration and air flow rate increased, the degradation rates decreased. Maximum VOC degradation rates of toluene, ethylbenzene, and chlorobenzene were obtained as 81%, 71%, and 92% by simultaneous adsorption and photocatalytic oxidation under UVA light at 30% RH and 30 °C, respectively. Chlorobenzene showed a higher removal efficiency than toluene and ethylbenzene for all conditions. The hydrophilic nature of the ZnO NR surface promoted the adsorption of chlorinated compounds. The interaction of VOCs with the catalyst surface revealed that surface chemistry plays a significant role in photocatalytic removal.

KEYWORDS: *environmental and catalysis application, flexible photocatalyst, ZnO, polyurethane foam, flexible, toluene, ethylbenzene, chlorobenzene*

1. INTRODUCTION

Volatile organic compounds (VOCs) are a significant environmental concern due to their adverse effects on air quality and human health. VOCs react with other pollutants to form harmful substances that contribute to ground-level ozone and photochemical smog formation. Additionally, a group of VOCs contributes to climate change through secondary organic aerosols. Long-term exposure to VOCs is linked to various health issues, including respiratory problems and cancer.[1,2] Increasing VOC emissions has led to the development of many technologies and strategies for their control. Advanced VOC control technologies include recovery processes such as adsorption, absorption, condensation, membrane separation, and degradation methods such as biofiltration, thermal oxidation, and photocatalytic oxidation (PCO).[3,4] Adsorption

Received: February 2, 2025
Revised: March 26, 2025
Accepted: March 27, 2025
Published: April 3, 2025

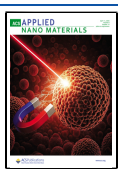

ACS Publications

© 2025 The Authors. Published by American Chemical Society

Downloaded from pubs.acs.org/aanmf6/article-pdf/8/14/7290/4068736/an5c00665.pdf by guest on 17 November 2026

acts as the initial step by concentrating VOC molecules onto the catalyst surface, thereby increasing the probability of reactive species interactions and subsequent oxidation.[5] PCO is one of the most effective removal methods that utilizes semiconductor catalysts and ultraviolet (UV) light to convert organic compounds into harmless and odorless products (e.g., H_2O and CO_2). The efficiency of photocatalysts is determined by their ability to accelerate light-induced reactions under various irradiation conditions.[6] Adsorption and PCO are two interrelated processes that play a crucial role in efficiently removing VOCs. This sequential mechanism involving molecular adsorption, catalytic transformation via surface-mediated redox reactions, and the desorption of reaction products emphasizes the correlation between adsorption and catalytic oxidation in optimizing VOC degradation pathways.[7] Among the numerous semiconductor photocatalysts (e.g., CuO, Fe_2O_3, Ag_2O, BiO_4, CeO_2, ZnO, and WO_3), TiO_2 and ZnO have been studied extensively.[8] Most studies on ZnO photocatalysts, which are nontoxic, cost-effective, and abundant alternatives to TiO_2, have been conducted only for the liquid phase photodegradation of dyes and pharmaceuticals.[9] A limited number of studies have been conducted using ZnO photocatalysts for the removal of hazardous VOCs. ZnO is a semiconductor characterized by a wide band gap (~3.37 eV) useful for ultraviolet detection, a large exciton binding energy (60 meV), and high electron mobility (~400 $cm^2\ V^{-1}\ s^{-1}$). Furthermore, the ability to design ZnO nanostructures with specific properties has created new possibilities to increase the efficiency of VOC removal via photocatalysis.[10,11]

The effective charge separation properties and band gap energies of photocatalysts are largely dependent on the crystal size and crystal phase. ZnO nanostructures [i.e., nanorods (NR), nanowires, nanosheets, nanoparticles, etc.] exhibit improved photocatalytic performance compared to bulk ZnO due to their high surface area, improved charge separation efficiency, and enhanced light harvesting ability.[12,13] One-dimensional (1D) nanostructures such as ZnO nanowires and NRs are highly favorable for charge carrier collection and transfer along the direction of nanostructure growth and are also effective in the separation of electron−hole pairs. 1D ZnO NRs with a high surface-to-volume ratio exhibit enhanced light absorption possibilities due to multiple light scattering and reflection.[14]

The immobilization of ZnO on polymer substrates leads to new avenues for designing advanced materials with specific functionalities and improved performance. ZnO/polymer hybrid structures offer synergistic effects by combining the flexibility and versatility of polymers with the catalytic and optical properties of ZnO.[15,16] Flexible photocatalysts expand the application range of photocatalytic systems by facilitating integration onto planar surfaces. Feng et al. designed a filter by growing ZnO NRs decorated with Ag having a hierarchical structure on the surface of PTFE nanofibers by the hydrothermal method for the removal of formaldehyde.[17] Chae et al. fabricated a hybrid visible photocatalyst utilizing an organic and inorganic p−n junction formed by self-assembled poly(3-hexylthiophene) nanomesh and ZnO NR for indoor air purification.[18] Among the polymer support materials, polyurethane (PU) foam is a prominent substrate due to its excellent mechanical properties, low density, chemical stability, lightweight structure, high surface area, and three-dimensional (3D) porous structure.[19] Combining PU foam with photocatalysts increases the available surface area for photocatalytic reactions and facilitates pollutant degradation. Understanding the surface chemistry is critical for determining the physicochemical properties of PU surfaces such as polarity, hydrophobic interactions, and van der Waals forces. Improved wettability of the surface is usually attributed to the presence of −OH functional groups.[20] Modified PU foams have been studied in many application areas such as photocatalytic water splitting, desalination by photothermal heating, photocatalytic degradation of organic pollutants, oil−water separation, and oil removal processes. Pham et al. reported a study on the photocatalytic removal of toluene in aerosol under visible light irradiation, using a photocatalyst synthesized by immobilizing V-doped TiO_2 on PU foam.[21] Freitas et al. examined the adsorption capacities of polar and nonpolar VOCs in composites of metal−organic frameworks within PU foams.[22] He et al. evaluated the microbial removal of toluene-containing flue gas by loading PU foams in twin bio trickling filters.[23]

In this study, a flexible hybrid photocatalyst for VOC removal was developed by growing ZnO NRs on PU foam substrates with a high surface area. A predictive evaluation of the performance of hybrid photocatalysts developed with innovative approaches for potential real-world and large-scale applications is provided. Commercially available PU foam surfaces were functionalized before the catalyst immobilization process through chemical solution treatment developed by using novel approaches. The PU/ZnO NR hybrid structure was developed by growing ZnO NRs on a seeded PU foam. The chemical processes were carefully designed to maintain the structural integrity and flexibility of the foam, while creating a hybrid structure. Photocatalytic experiments were conducted in a plug flow type reactor, where the reactant was perfectly mixed in the radial direction but not in the axial direction (forward or backward). Toluene, ethylbenzene, and chlorobenzene were selected as model VOCs due to their structural similarities to aromatic hydrocarbons but distinct functional groups, influencing their adsorption and photocatalytic degradation. These compounds are widely emitted from industrial sources and are classified as priority pollutants, making their removal crucial for environmental protection.[24,25] In the presence of a PU/ZnO NR hybrid structure, the adsorption and PCO behaviors of toluene, ethylbenzene, and chlorobenzene were determined under light-off and UVA light conditions, respectively. Parameters affecting the performance of the PCO process, such as the VOC concentration, gas flow rate, relative humidity (RH), and temperature, were comprehensively evaluated. Furthermore, semiconductor photocatalyst design and optimization strategies were discussed to enhance the efficiency and sustainability of PCO for VOC removal.

2. EXPERIMENTAL METHODS

2.1. Materials. A commercially produced polyester-based PU foam sheet (Recticel) was cut into cylindrical pieces (4.5 cm diameter; 4 cm height) for use as flexible substrates. The PU foam surface, which is hydrophobic, was activated by chemical solution treatment with hexamethylene diisocyanate (HDI) ($C_6H_{12}N_2O_2$, Sigma-Aldrich), dibutyltin dilaurate (DBDTL) ($C_{32}H_{64}O_4Sn$, 95%, Sigma-Aldrich), and toluene ($C_6H_5CH_3$, Supelco). Zinc acetate dihydrate (ZAD) ($C_4H_6OZn{\cdot}6H_2O$, Merck) salt was dissolved in ethanol (C_2H_5OH, 99%, Merck) as a Zn^{2+} ion source for the deposition of the ZnO thin film. The pH of the solution was adjusted to ~10 with dilute sodium hydroxide (NaOH, Merck) solution. Zinc nitrate hexahydrate (ZNH) ($Zn(NO_3)_2{\cdot}6H_2O$, Sigma-Aldrich) and hexamethylenetetramine (HMTA) ($C_6H_{12}N_4$, Merck) were used as Zn^{2+} and OH^- ion sources in the aqueous CBD precursor solution, respectively. Acetone (C_3H_6O, Merck) was used for washing purposes. Toluene ($C_6H_5CH_3$, Supelco),

Downloaded from pubs.acs.org/aanmf6/article-pdf/8/14/7290/4068736/an5c00665.pdf by guest on 17 November 2026

https://doi.org/10.1021/acsanm.5c00665
ACS Appl. Nano Mater. 2025, 8, 7290−7303

Scheme 1. Schematic Illustration of the Structure Design and Synthesis Process [Surface Modification (a), Seed Deposition (b), and NR Growth (c)] from a Chemical Perspective

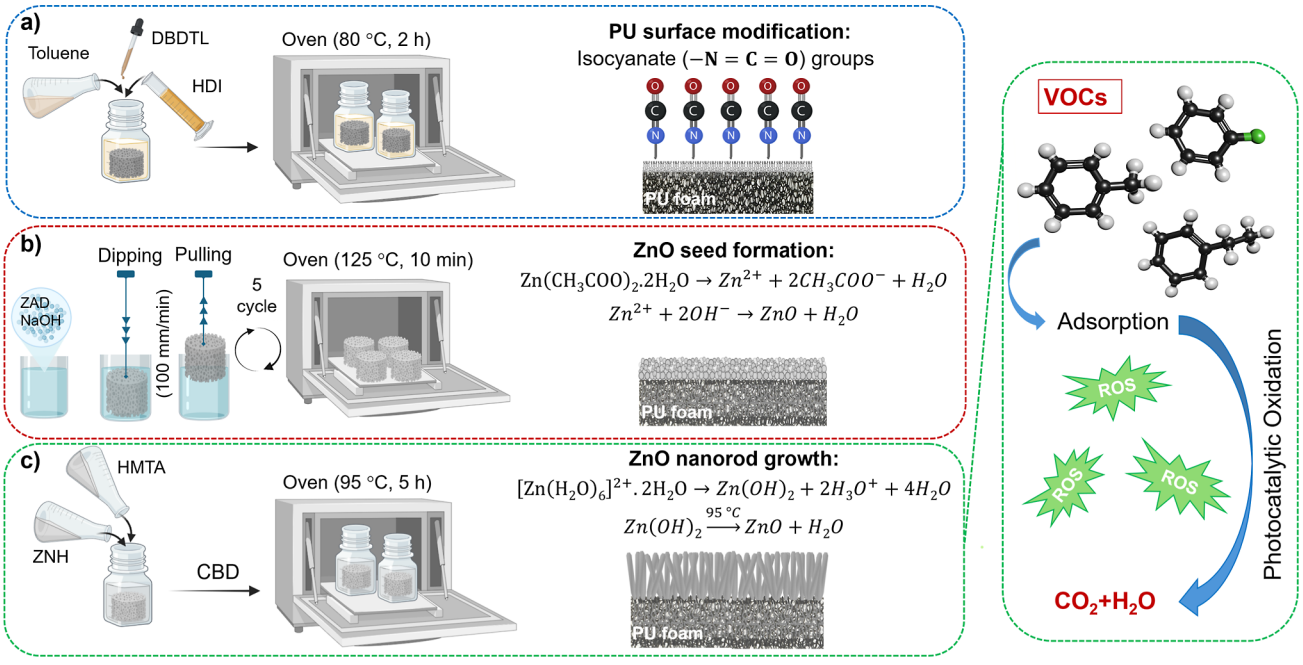

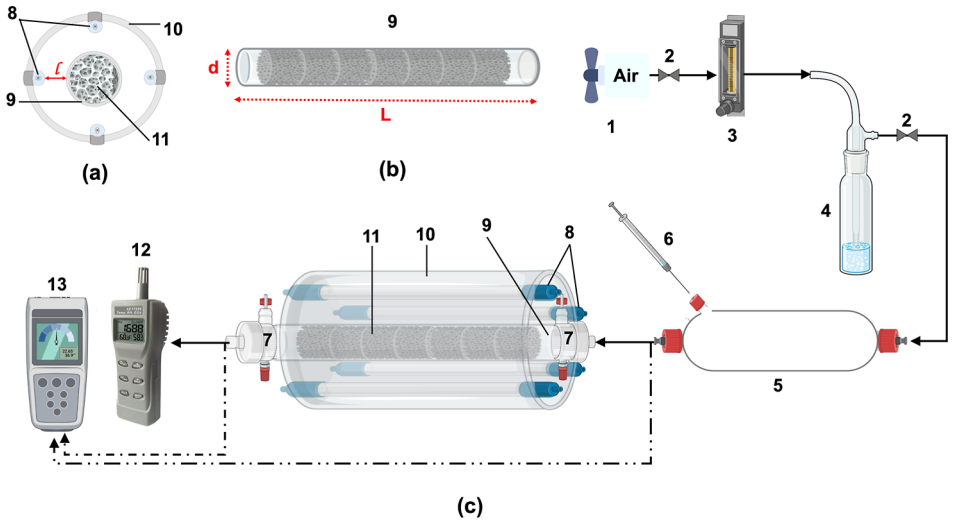

Figure 1. Schematic illustration of the cross-sectional top view of PFR (a), the cross-sectional side view of PFR (b), and plug flow PCO reactor setup (c) [1-air valve, 2-flowmeter, 3-control valve, 4-humidifier, 5-gas mixture bottle, 6-injector, 7-glass faucet, 8-UV lamps, 9-Pyrex-glass tube, 10-plexiglass reactor, 11-catalysts, 12-gas detector ($VOCs/CO_2$), and 13-thermometer and hygrometer].

chlorobenzene ($C_6H_5CH_3$, Merck), and ethylbenzene ($C_6H_5CH_3$, Sigma-Aldrich) were used as model VOCs.

2.2. Production of a Flexible Hybrid Catalyst. Surface modification is required to make the hydrophobic PU foam suitable for chemical bonding. The cylindrical PU foams were treated in the solution prepared by dissolving HDI and DBDTL in toluene at a volume ratio of 0.05/0.0025/1, respectively. The foams, immersed in the solution, were consecutively treated in an oven at 80 °C for 2 h, washed with toluene, and dried by air. HDI treatment aimed to enrich the PU surface with isocyanate (−N═C═O) groups. A thin seed layer was deposited on the PU foams to grow well-aligned ZnO NRs. Therefore, 0.1 mL of ZAD was dissolved in 100 mL of ethanol to prepare a seed solution, and the pH was adjusted to ∼10.5 by using a 0.1 M NaOH solution. The solution was continuously stirred at 60 °C for 2 h to facilitate the formation of ZnO through the thermal dehydration of the zinc salt. Subsequently, the ZnO seed layer was deposited onto the PU foam surfaces using a multistep dip-coating process repeated five times at a fixed pulling speed of 100 mm/min. Each dipping step was followed by drying at 125 °C for 10 min to ensure uniform adhesion between seed and PU foam. The ZnO NRs were grown on the preseeded surfaces utilizing a low-temperature chemical bath deposition (CBD) method. An aqueous precursor solution containing equimolar amounts of 0.5 M ZNH and HMTA was prepared for the CBD process. The seeded PU foams were suspended in the precursor solution in a glass beaker maintained at 95 °C for 5 h. At the end of the growth process, the samples underwent thorough rinsing with acetone, followed by multiple rinses with deionized (DI) water before being left to air-dry. Then, the PU/ZnO NR hybrid photocatalysts were heated in an oven at 150 °C for 30 min to remove excess water and solvents. A schematic illustration presenting the system and the synthesis process from a chemistry perspective is shown in Scheme 1.

https://doi.org/10.1021/acsanm.5c00665
ACS Appl. Nano Mater. 2025, 8, 7290−7303

Downloaded from pubs.acs.org/aanmf6/article-pdf/8/14/7290/4068736/an5c00665.pdf by guest on 17 November 2026

2.3. Photocatalytic Experiments. The photocatalytic experiments were carried out in a plug flow reactor made of Pyrex-glass. The reactor geometry is designed to be cylindrical with a volume of ∼0.5 L (π*2.25^2*30 cm^3). The Pyrex-glass tube is placed horizontally at the center of the plexiglass reactor stand at an equal distance (l = 7 cm) from the light sources. A light assembly consisting of 4 actinic UVA lamps (Philips Actinic BL 8 W) was fixed around the inner wall of plexiglass stand with equal distance between them. The light intensity of the lamps was measured as 2.54 mW/cm^2 with Lutron UVA-365SD. A UVA Light Meter with a probe was placed at the center of the light source during measurement. Flexible hybrid PU/ZnO NR catalysts were designed in cylindrical geometry with a diameter of 4.5 cm and a length of 4 cm. For each experimental set, seven catalyst samples were put in the Pyrex-glass tube without leaving any space between them to ensure that the gas effectively reached the entire surface of the catalysts. A schematic illustration of the plug flow type PCO reactor setup is given in Figure 1.

The inlet of the Pyrex-glass reactor is connected to the gas mixture bottle (500 mL) for gas transfer. Liquid ethylbenzene, chlorobenzene, and toluene, injected into the gas mixture bottle, were converted to the gas phase by the synthetic air from the compressed air line. The residence time of the gas was determined according to the flow rate. The flow rate of the air transferred to the system was adjusted to 1 (FR_1), 0.6 (FR_2), and 0.3 (FR_3) L/min by the flowmeter. The gaseous-phase VOCs were directly supplied to the system through a pipe. The reactor outlet was directly connected to a gas detector. Concentrations of toluene, dichloromethane, ethylbenzene, and CO_2 (as the product of oxidation reaction) during the adsorption and PCO were detected with Dräger X-am 8000 detectors at diffusion mode, using a PID LC ppb detector for VOCs and IR detector for CO_2 with a detection range of 0−5 vol % CO_2. The gas concentrations were adjusted by injecting fixed liquid volumes of 0.2, 0.4, and 0.6 μL of toluene, chlorobenzene, and ethylbenzene. The feed concentrations corresponding to VOCs volumes were calculated using the ideal gas equation and expressed in parts per million (ppm), as listed in Table S1 (see the Supporting Information file). For a 0.2 μL injection, the gas concentrations were determined to be 43.3 ppm for toluene, 45.8 ppm for ethylbenzene, and 43.3 ppm for chlorobenzene. Similarly, the concentrations corresponding to 0.4 μL were 86.6 91.6, and 86.6 ppm, while these values were 129.9, 137, and 129 ppm for 0.6 μL, respectively. The effects of four different parameters, namely, pollutant concentration, RH, temperature, and gas flow rate on photodegradation efficiency, were investigated for three different model molecules. The evaluated conditions are listed in Table 1. All experiments, regardless of the temperature parameter, were performed under ambient pressure conditions at room temperature (21 ± 2 °C). The Pyrex-glass tube was heated with a heating unit to investigate the effect of the temperature on the photocatalytic degradation rates. Removal efficiencies at different temperatures (21, 25, 30, and 35 °C) for constant concentration (C_{F2}) and flow rate (FR_2: 0.6 L/min) were determined for three model pollutants. The inlet air humidity was adjusted by passing dry air through DI water in a gas-washing bottle connected to the gas mixed bottle. The humidity was adjusted by controlling the evaporation rate of the DI water in a water bath. The RH and gas temperature were monitored using a thermometer and a hygrometer at the photoreactor inlet. Photocatalytic experiments for constant gas concentration and flow rate at different RH rates (0, 15, 30, 45, and 65%) were carried out for all three model pollutants.

Table 1. List of Evaluated Photocatalytic Experimental Conditions

VOCs	volume (μL)	flow rate (L/min)	temperature (°C)	RH (%)
toluene	CF_1: 0.2	FR_1: 1	21	0
ethylbenzene	CF_2: 0.4	FR_2: 0.6	25	15
chlorobenzene	CF_3: 0.3	FR_3: 0.3	30	30
			35	45
				65

The stability of flexible photocatalysts was evaluated by performing five consecutive tests at a constant VOC concentration (C_{F2}) and constant flow rate (FR_2) for three molecules after the cleaning cycle. The cleaning process was carried out by passing the humid air under UVA irradiation and keeping it in the oven at 70 °C for 2 h to ensure thorough removal of possible byproducts adsorbed on the photocatalyst surface. The photocatalytic experiments were carried out under steady-state conditions, involving two main mechanisms. The first mechanism involves the adsorption of pollutant molecules onto the photocatalyst surface under dark conditions. The second mechanism involves a series of PCO reactions that occur on the catalyst surface in the presence of molecules under UVA light. Furthermore, photolysis experiments attributed to the degradation of molecules by light in the absence of catalysts were also conducted. Adsorption experiments are generally associated in the literature with establishing adsorption−desorption equilibrium in the reactor system in the literature. Relatively low concentrations were investigated in the study to simulate real-world conditions. Considering that the plug-flow reactor is fed only once and a high surface area is offered by the flexible nanohybrid structure, reaching adsorption−desorption equilibrium for low concentrations is challenging. Therefore, instead of a fed system, a continuous flow system was designed for adsorption experiments, as shown schematically in Figure S1 (see the Supporting Information file). In this system, VOCs were not injected into the 500 mL gas mixture bottle that supplied gas to the reactor. 1 mL of the liquid model molecule was added to an additional 100 mL gas mixture bottle. The pollutant in the gas phase was then transferred to the main gas mixture bottle with a syringe by evaporation at a constant flow rate and room temperature (21 °C). Thus, the rate at which the inlet concentration reaches the outlet concentration (catalyst saturation) was monitored by continuously feeding the reactor at a constant concentration. First, control experiments (i.e., without catalyst) and adsorption experiments were carried out using PU/ZnO NR hybrid catalysts for three model pollutants at different flow rates (FR_1, FR_2, and FR_3). PCO reactions were initiated by direct irradiation, considering that adsorption−desorption had reached equilibrium over long periods. Furthermore, control experiments were conducted to assess the structural stability of the PU foam under UV irradiation. Untreated PU foams were placed in the reactor, and the CO_2 concentrations were monitored under light-on conditions for 180 min. The degradation rates and removal efficiencies of VOCs were calculated over time (1, 2), where C_0 and C_t represent the initial and time-specific VOC concentrations (ppm) adjusted according to controlled parameters.

$$\text{VOC degradation rate}\left(\frac{\text{ppm}}{\text{min}}\right) = \frac{(C_0 - C_t)}{\Delta t} \quad (1)$$

$$\text{VOC removal efficiency} = \frac{C_0 - C_t}{C_t} \times 100 \quad (2)$$

The kinetics of photocatalytic reactions were determined by first-order kinetic modeling. A first-order reaction is dependent on the concentration of only one reactant. The rate-determining step for a first-order reaction is calculated based on the degradation rates up to the first 8 min by the following equations

$$C_t = C_0 e^{-kt} \quad (3)$$

$$\ln\left(\frac{C_t}{C_0}\right) = -kt \quad (4)$$

where k represents the rate constant or kinetic constant of the reaction. The slope of the time-dependent $\ln(C_t/C_0)$ curve thus obtained gives the kinetic constants (k, min^{-1}), and the related correlation coefficients (R^2) were also determined.

2.4. Characterization. The functional groups and intermolecular bond structures of the ZnO/PU nanohybrid structure for all production steps were determined by FT-IR (PerkinElmer Spectrum 100). The

Downloaded from pubs.acs.org/aanmf6/article-pdf/8/14/7290/4068736/an5c00665.pdf by guest on 17 November 2026

https://doi.org/10.1021/acsanm.5c00665
ACS Appl. Nano Mater. 2025, 8, 7290−7303

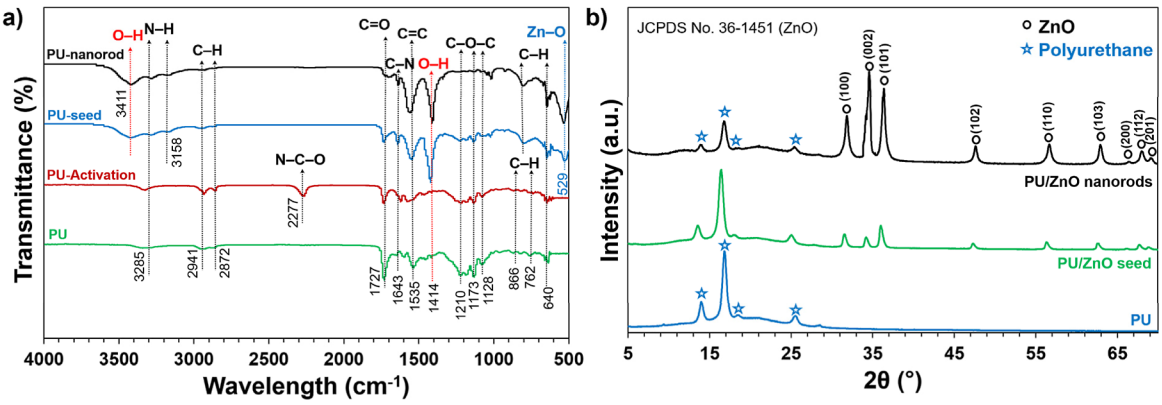

Figure 2. (a) FT-IR spectra of untreated (PU), activated (PU-Activation), ZnO seeded (PU-seed), and ZnO NRs-grown (PU-NR) PU foams and (b) XRD patterns of untreated, ZnO seeded, and ZnO NRs-grown PU foams.

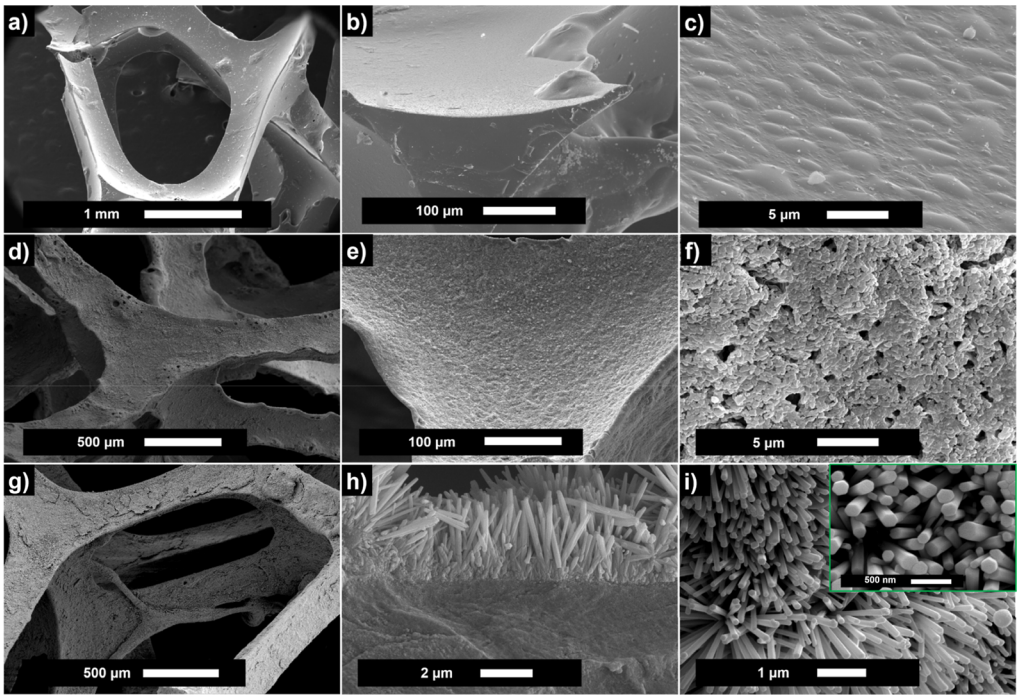

Figure 3. SEM micrographs of untreated (a–c) and ZnO seeded (d–f) and ZnO NRs-grown (g–i) PU foams at different magnifications.

crystallographic structures of bare, ZnO seeded, and ZnO NRs grown on PU foams were investigated using an X-ray diffractometer (Rigaku D Max 200) with Cu Kα radiation in the 2θ range from 5 to 70°, with a scanning rate of 2 min^{-1}. The morphologies and elemental analyses of all these samples were examined by SEM (Philips XL30SFEG) with energy-dispersive X-ray spectrometry (EDS). The ultraviolet/visible (UV–vis) light absorbance and reflectance measurements of ZnO NRs were characterized by a spectrophotometer (UV–vis, Shimadzu 2101), and the room temperature photoluminescence (PL) property was investigated by a spectrofluorometer (Varian Eclipse) using a xenon lamp with an excitation wavelength of 350 nm, as detailed in previous studies.[26,27]

3. RESULTS AND DISCUSSION

3.1. Materials Characterization. The surfaces of the PU foam were functionalized through chemical solution treatment to enhance their bonding ability and hydrophilicity. The functional groups present on bare, ZnO-seeded, and ZnO NR-grown PU foams were identified by FT-IR analysis at room temperature. The FT-IR spectra of all samples in the wavenumber range of 4000–500 cm^{-1} are shown in Figure 2a. The bands attributed to the symmetrical bending and stretching vibrations of the N–H groups of PU are located at 3285 and 1512 cm^{-1}. The bands at 2941 and 2872 cm^{-1} are due to stretching vibrations of the C–H groups in the methyl and methylene segments, indicating the presence of soft segment polyether polyols.[19,28] The band located at 1727 cm^{-1} represents the stretching vibrations of the C═O carbonyl in the urethane group. The band at 1643 cm^{-1} is related to the C–N bonds. The strong absorption peak at 1535 cm^{-1} is associated with the C═C bond vibrations in the benzene ring. The C–O–C ether bonds produce relatively broad and strong bands at 1173 and 1128 cm^{-1}. The weak absorption peaks at 866 and 752 cm^{-1} are attributed to the stretching vibrations of the C–H bonds.[29] Following the activation process, a new peak at 2277 cm^{-1}, related to the tensile vibrations of the −N═C═O− isocyanate groups, confirms the successful covalent binding of HDI (hexamethylene diisocyanate) to the PU surface.[30] The spectra of the ZnO seeded and NR-grown PU foams (i.e., PU/ZnO

https://doi.org/10.1021/acsanm.5c00665
ACS Appl. Nano Mater. 2025, 8, 7290–7303

Downloaded from pubs.acs.org/aanmf6/article-pdf/8/14/7290/4068736/an5c00665.pdf by guest on 17 November 2026

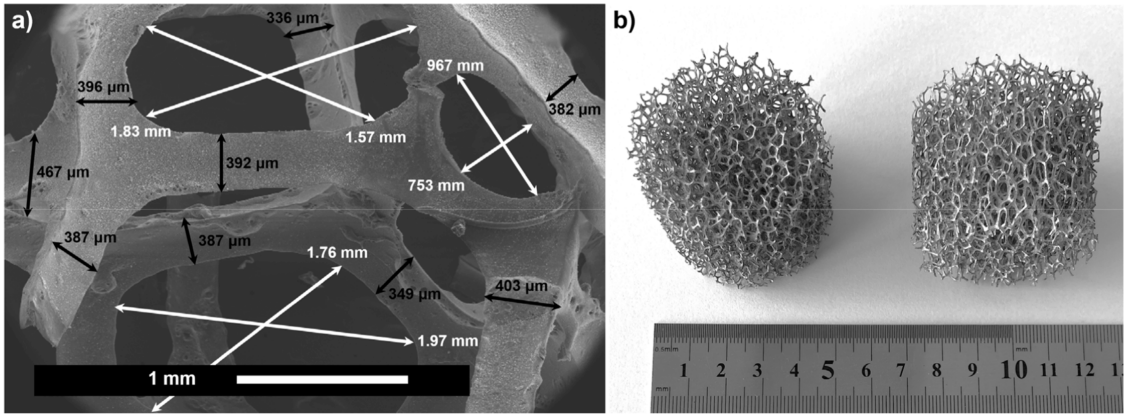

Figure 4. SEM micrograph of PU foam showing window size and strut diameter measurements (a) and optical image of the PU/ZnO NR hybrid catalyst (b).

NRs) exhibit a strong absorption band located at 529 cm^{-1}, corresponding to the Zn−O bond, which aligns with metal−oxygen frequencies reported in the literature.[31] Furthermore, the signals observed at 3411 and 1414 cm^{-1} were assigned to the stretching and bending vibrations of the O−H bonds, respectively, corresponding to water adsorption on the metal-hydroxide layers.[29,32] These outcomes substantiate the chemical bonding of the ZnO NRs to the PU foam surface.

The crystal structures of untreated, ZnO seeded, and ZnO NR-grown PU foams examined by XRD are shown in Figure 2b. All diffraction peaks correspond to the standard diffraction patterns of the hexagonal wurtzite phase of ZnO (JCPDS no. 36-1451) and those of PU. The PU foam exhibits strong diffraction peaks at 2θ values of 17.1, 14.2, 18.7, and 26.3°. The ZnO diffraction peaks are observed at 2θ values of 31.7, 34.4, and 36.2°, corresponding to the (100), (002), and (101) planes, respectively.[33,34] The most intense diffraction peak, corresponding to the (002) plane, is evidence of the preferential alignment of the NRs along the *c*-axis. Furthermore, the XRD pattern of the photocatalyst sample (i.e., PU/ZnO) still shows prominent peaks from the PU phase. Despite the thin photocatalyst layer, the diffraction peaks are quite sharp and intense, confirming the crystallization of the ZnO.

The morphologies of untreated and nanohybrid structures were examined in detail by using scanning electron microscopy (SEM), and the SEM micrographs are shown in Figure 3. The surface of the untreated PU foam is slightly rough with network struts exhibit a triangular concave geometry. The ZnO seed layer, serving as a nucleation site for the formation of ZnO NRs, was homogeneously deposited on the modified PU substrate surfaces (Figure 3e). The seeds are spherical in shape with a grain size distribution at submicron levels. The seed layer remains robust and free from delamination on the modified PU surface, indicating that the chemically modified PU surface provides active hydroxyl groups that facilitate ZnO nucleation. The ZnO NRs have a hexagonal cross-section as shown by the high-magnification SEM image added as an inset Figure 3i and are predominantly aligned vertically at the centers of seeds.

The estimated average thickness of the ZnO seed layer and average length of the ZnO NRs are approximately 0.3 and 1.2 μm, respectively, as determined from SEM micrographs. Flexible PU foam decorated with ZnO NRs offers several advantages for degradation processes by facilitating effective interaction with UV radiation due to its highly porous structure as well as providing pathways for liquid flow through millimeter-scale open windows between neighboring cells. The high specific surface area of the NRs, combined with the 3D reticulated structure, provides the efficient adsorption of pollutant molecules on both the inner and outer surfaces of the photocatalyst, thereby enhancing the photocatalytic performance. Moreover, elemental analysis was performed by using EDS to verify the composition of the PU/ZnO hybrid structure. The EDS spectra and elemental compositions of untreated, activated, and ZnO NRs-grown PU foams are presented in Figure S2 (see the Supporting Information file). The observed increase in the nitrogen (N) atomic percentage following the PU surface modification step was attributed to the presence of isocyanate groups (−N═C═O−). The Zn-to-O ratio was determined to be ∼43:33 (at. %), consistent with our previous studies indicating Zn-rich ZnO NRs due to Zn^{2+}-terminated upper surfaces. Therefore, the stoichiometry is represented as ZnO_x, where $x < 1$.[28]

The macroscale characteristics of the PU foams were determined in terms of strut diameter (d_s) and window size (α) using the lengths measurement from the SEM micrograph (Figure 4a), and the values are listed in Table 2. These values represent the arithmetic mean of 10 measurements including their standard deviations. The average open porosity (ε) of the PU foams was calculated using the relative total volume of the cylindrical sample (V_T) ($V_T = \pi(2.25)^2 \times 4$ cm^3) and the theoretical density of the PU. This porosity is essentially the ratio of the theoretical volume derived from the sample mass to the (V_T) value. In a similar manner, the average specific volume of the foam samples is calculated as the ratio of (V_T) values to their relevant masses. The following equation was used to calculate the specific surface area (A_s) per unit volume of the PU foam structure with triangular concave struts (Figure 3b)[35]

$$A_s = \left\lceil \frac{((1 - 0.971)(1 - \varepsilon))^{0.5}}{(\alpha(1 - \varepsilon))^{0.5}} \right| \quad (5)$$

Table 2. Macroscale Properties of PU Foam

strut diameter (d_s)	340 ± 50 μm
window size (α)	1734 ± 280 μm
theoretical density of polyurethane	0.3 ± 0.002 g cm^{-3}
open pore (ε)	%90
specific surface area (A_s)	466.23 m^{-1}

Downloaded from pubs.acs.org/aanmf6/article-pdf/8/14/7290/4068736/an5c00665.pdf by guest on 17 November 2026

https://doi.org/10.1021/acsanm.5c00665
ACS Appl. Nano Mater. 2025, 8, 7290−7303

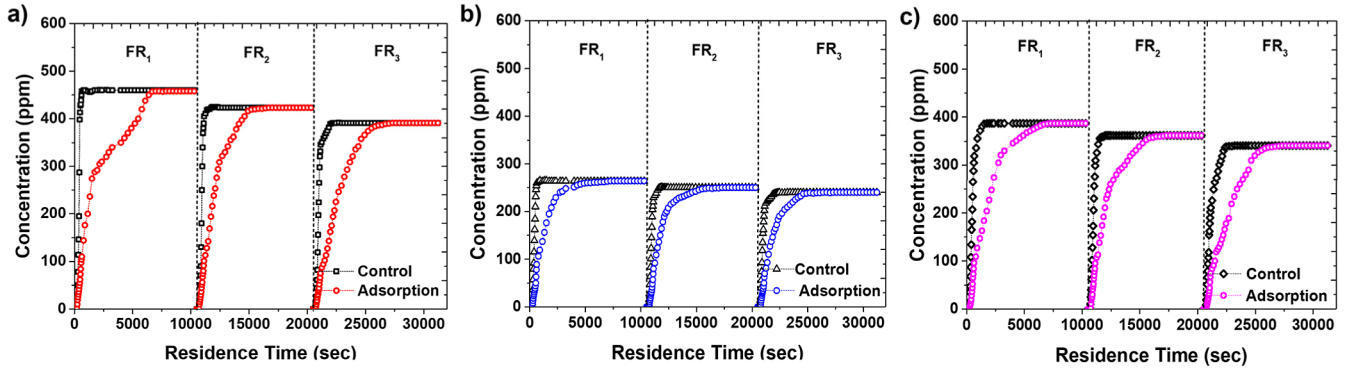

Figure 5. Concentration changes of toluene (a), ethylbenzene (b), and chlorobenzene (c) for control (i.e., no catalyst) and adsorption experiments using PU/ZnO NR hybrid catalysts under dark conditions.

where A_s is the specific surface area of the PU foams. Each photocatalytic degradation experiment utilized seven cylindrical photocatalyst samples, with their average total weight being ~13.464 g, corresponding to a specific surface area of approximately 0.36 m^2.

The optical image of the designed flexible PU/ZnO NR hybrid sample is shown in Figure 4b. The cylindrical-shaped PU foam maintained its structural integrity, size, and flexibility. The ZnO NRs were homogeneously distributed on all struts and wall, and the successful activation of the PU foam was confirmed. Moreover, the PU foam turned grayish due to the multiple light scattering ability of the ZnO NRs. The optical characterization of ZnO NRs was comprehensively performed in a previous study, where UV−visible and PL analyses were conducted on samples grown under identical conditions. The results demonstrated a band gap energy of 3.22 eV, lower than bulk ZnO (3.37 eV), attributed to defect-induced broadening, while PL analysis confirmed strong excitonic recombination with a prominent UV emission at ~388 nm.[26,27]

3.2. Photocatalytic Degradation of VOCs. The removal of pollutants by PCO processes involves three main steps: first, the transfer from the bulk of the catalyst to its surface (external and internal mass transfer); second, the adsorption of pollutant molecules onto the catalyst surface; and finally, the mineralization of pollutants through the decomposition into intermediate products by reactive species on the active sites of the surface. The performance of a photocatalytic reactor is controlled by three main parameters: the VOC convective mass transfer, reaction rate, and irradiated reaction surface area. However, these parameters depend on various factors. The irradiated reaction surface area and VOC convective mass transfer are influenced by the catalyst configuration and reactor geometry, while the latter is also affected by the physical properties of the pollutants and flow rate. The degradation rate depends on the physical and chemical properties of the pollutant, UV light intensity, reaction temperature, and humidity level.[36,37] This study investigates the effects of pollutant type, initial pollutant concentration, synthetic air flow rate, reactor temperature, and RH on the photocatalytic performance. Control and photolysis experiments were carried out (i.e., without catalysts) to clarify the performance of the developed flexible PU/ZnO NR hybrid structure. Control and photolysis experiments were conducted under dark conditions and UVA radiation, respectively. The time-dependent concentration change curves for toluene, ethylbenzene, and chlorobenzene are shown in Figure S3 (see the Supporting Information file). In the absence of a catalyst material, there is no direct degradation of VOC molecules by UVA light (i.e., photolysis).

3.2.1. Adsorption Mechanism. The nanohybrid structures are expected to exhibit high adsorption capacities due to the 3D network structure of the PU foam combined with the high surface area provided by the ZnO NR structure. Adsorption experiments in the literature are commonly associated with the establishment of an adsorption−desorption equilibrium in the reactor system. This equilibrium is defined as the point at which the inlet gas concentration equals the outlet gas concentration. In this study, relatively low concentrations were used to approximate the real-world conditions. A continuous gas flow with a constant concentration was supplied to ensure that the catalyst reached its saturation point, overcoming the challenge of achieving adsorption−desorption equilibrium in a single-feed plug flow reactor. Each adsorption experiment was conducted under dark conditions in a continuous-flow reactor design and lasted approximately 2 h. The time-dependent changes in concentration for adsorption in both control experiments (i.e., no catalyst) and in the presence of a catalyst for the three pollutants are shown in Figure 5. Due to the different evaporation temperatures of toluene, ethylbenzene, and chlorobenzene, the concentrations observed in control experiments differ from the calculated theoretical values. Ethylbenzene has the highest evaporation temperature, resulting in a lower equilibrium concentration. The equilibrium concentrations increased with the flow rate for all pollutants. A higher flow rate acts as a driving force, allowing more gas molecules to pass through the system. Furthermore, a higher input VOC concentration gradient led to an increased adsorption rate. However, at high flow rates, the model VOCs may pass through the reactor without fully interacting with the catalyst. The findings revealed that the total mass of VOCs adsorbed on the catalyst surface was higher at lower flow rates. The effect of the flow rate should be evaluated in consideration of the reactor geometry. In ideal plug-flow reactors, the time required for gas-phase molecules to adsorb onto the surface is a critical factor. The length-to-width ratio of the reactor plays a crucial role in this process, and this ratio should be > 20 for ideal gas diffusion. The laboratory-scale reactor used in this study has a length-to-width ratio of ~6.6. Quici et al. reported that a reactor length of 10 cm provided a removal efficiency significantly higher than 5 cm for the low concentrations at the same flow rate. However, doubling the reactor length with equal residence times and varying the toluene concentration resulted in only a slight improvement in degradation rates. This indicated that ideal flow and mixing behavior, probably due to some outgassing before

Downloaded from pubs.acs.org/aanmf6/article-pdf/8/14/7290/4068736/an5c00665.pdf by guest on 17 November 2026

https://doi.org/10.1021/acsanm.5c00665
ACS Appl. Nano Mater. 2025, 8, 7290−7303

the catalyst was fully saturated.[38] In this study, although flow rates were adjusted to optimal levels, the results were evaluated by considering the reactor geometry.

The adsorption capacities for all three pollutants were determined by comparing the areas under the control and adsorption curves. Under steady-state reaction conditions, catalyst saturation for toluene was achieved in 110 min at 450 ppm, while for chlorobenzene and ethylbenzene, it occurred after approximately 100 min at 385 and 285 ppm, respectively. The adsorption efficiencies of PU/ZnO NR hybrid structures for toluene, chlorobenzene, and ethylbenzene were found to be 22%, 19%, and 15%, respectively. For all pollutants, adsorption efficiencies decreased slightly with increasing flow rates.

3.2.2. Effect of Initial Concentration on PCO of VOCs. The high surface area provided by the PU/ZnO NR hybrid structure requires a relatively long time for the catalyst to reach saturation. Therefore, oxidation experiments were conducted in the plug-flow reactor system by simultaneous adsorption-oxidation mechanisms. Photocatalytic experiments were carried out under UVA irradiation at room temperature (21 °C) and using dry synthetic air (RH: 0%). Irradiation was simultaneous with the injection of a liquid pollutant into the reactor. PCO reactions for toluene, ethylbenzene, and chlorobenzene with three different initial concentrations (C_{F1}, C_{F2}, and C_{F3}) at a constant flow rate (FR_2) were confirmed by observing a significant decrease in pollutant concentrations. For all three pollutants, the degradation rate is inversely proportional to the initial concentration, as shown in Figure 6. The maximum

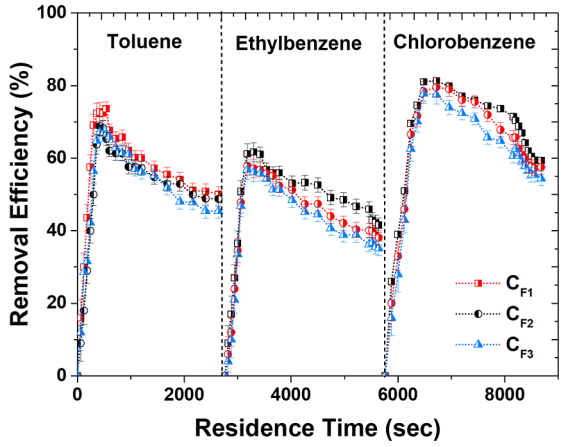

Figure 6. Removal efficiencies of toluene, ethylbenzene, and chlorobenzene with different initial concentrations (C_{F1}, C_{F2}, and C_{F3}) using PU/ZnO NR hybrid samples under UVA light irradiation.

removal efficiencies determined for toluene, ethylbenzene, and chlorobenzene were obtained for the lowest concentration values (C_{F1}). However, the maximum removal efficiencies were determined as 75% for toluene, 63% for ethylbenzene, and 81% for chlorobenzene. The removal efficiencies decreased slightly with increasing initial concentrations. In heterogeneous photocatalytic processes, bulk mass transfer is an important factor. At low inlet concentrations, degradation follows first-order kinetics, meaning that the degradation rate is proportional to the inlet concentration. In this case, the rate-limiting steps are either the adsorption or the transfer of the pollutant to the catalyst. Not all photoactive sites are occupied, and increasing the bulk concentration results in a higher surface concentration, thereby increasing the degradation rate. At higher inlet concentrations, the degradation rate tends toward a limit. In this case, the active sites are saturated, and increasing the concentration does not increase the degradation rate.

For photocatalytic reactions at the solid−gas interface, the frequency of molecular collisions between radicals and VOCs has the greatest effect on the degradation efficiency. Photocatalytic reactions initiated by the light excitation of pollutant molecules interacting with the catalysts generate hydroxyl ($^{\bullet}OH$) and superoxide anion ($^{\bullet}O_2^-$) radicals. Under steady operating conditions, the quantity of these radicals ($^{\bullet}OH$ and $^{\bullet}O_2^-$) remains constant. Thus, at higher initial concentrations, VOCs receive less photoelectric energy, leading to a slightly reduced degradation efficiency.[39] Most studies have concluded that increasing the pollutant concentration leads to a decrease in the removal efficiency of pollutants.[40] Rezaee et al. reported that increasing the toluene concentration results in a decrease in the photocatalytic efficiency of TiO_2 nanoparticles.[41] Chen et al. showed that the benzene removal efficiency by $BiVO_4/\alpha$-Fe_2O_3 composite decreased from 67% to 34% when the concentration was increased from 100 to 600 mg/m^3.[42] Excessive pollutant molecules on the photocatalyst surface may also prevent the adsorption of optical photons by the catalyst. Therefore, under constant irradiation, active oxidant species such as $^{\bullet}OH$ and $^{\bullet}O_2^-$ radicals are insufficient for the PCO of high pollutant concentrations.[39] The reaction kinetics were evaluated for the first 8 min when the removal efficiency reached its maximum.[37] The plot of $\ln(C/C_0)$ versus time is shown in Figure S4 (see the Supporting Information file). The kinetic constants (k) and associated correlation coefficients (R^2) were determined from the slopes of these curves. The maximum kinetic constant (k) for toluene, ethylbenzene, and chlorobenzene obtained for the low initial concentrations (C_{F1}) were 0.0031, 0.0023, and 0.0038 min^{-1}, respectively. Moreover, correlation coefficients (R^2) related to kinetic values were 0.95, 0.95, and 0,93.

3.2.3. Effect of Flow Rate on PCO of VOCs. Considering the reactor volume and inlet flow rates, the empty bed contact times were approximately 40, 35, and 30 min for flow rates of 0.3, 0.6, and 1 L/min, respectively. The time-dependent degradation rates for toluene, ethylbenzene, and chlorobenzene for constant concentration (C_{F2}) and different flow rates are shown in Figure 7. The highest removal efficiencies for toluene, ethylbenzene, and chlorobenzene were obtained at the lowest flow rate (FR_3:

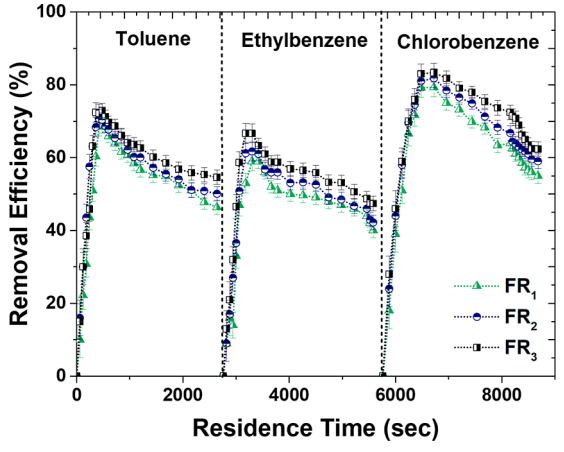

Figure 7. Removal efficiencies of toluene, ethylbenzene, and chlorobenzene with different air flow rates (FR_1, FR_2, and FR_3) using PU/ZnO NR hybrid samples under UVA light irradiation.

Downloaded from pubs.acs.org/aanmf6/article-pdf/8/14/7290/4068736/an5c00665.pdf by guest on 17 November 2026

https://doi.org/10.1021/acsanm.5c00665
ACS Appl. Nano Mater. 2025, 8, 7290−7303

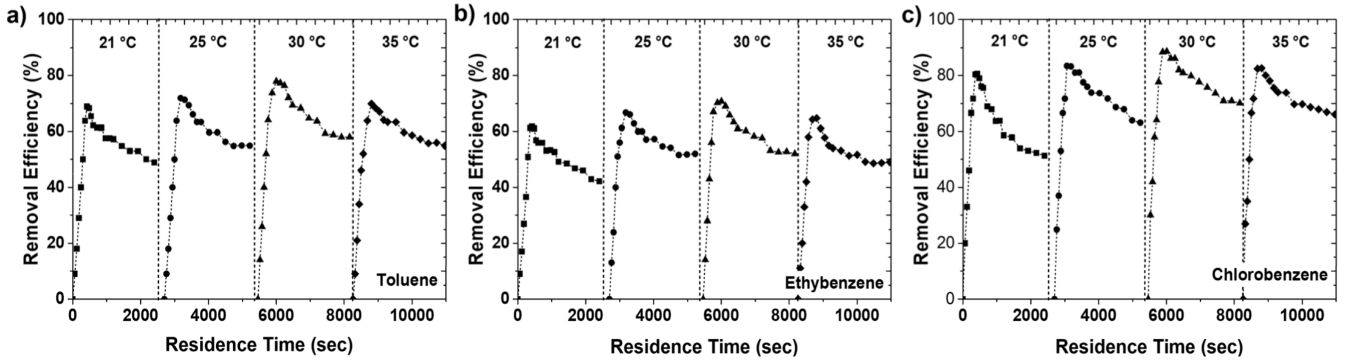

Figure 8. Effect of reaction temperature on removal efficiencies of toluene (a), ethylbenzene (b), and chlorobenzene (c) for PU/ZnO NR hybrid samples under UVA light irradiation.

0.3 L/min). The maximum removal efficiencies were 74% for toluene, 64% for ethylbenzene, and 83% for chlorobenzene. The maximum efficiency was reached in the first 8 min, and the removal efficiency gradually decreased partially until a pseudosteady state was reached. The accumulation of possible byproducts formed at the initial stage on the photocatalyst surface may compete with the adsorption of VOCs and thus slow down the photocatalytic reactions. On the other hand, for lower flow rates (0.3 L/min), the gas recirculation occurs more slowly, providing additional time for the photodegradation and desorption of the adsorbed byproducts. In plug-flow reactor systems, the flow rate can be defined as the residence time of the gas in the reactor. The low removal efficiency at high flow rates can be attributed to the reduced interaction time between VOC molecules and the catalyst surface.[43] The decrease in photocatalytic activity with the increase in the inlet flow rate of synthetic air is related to the lower bulk mass transfer (due to convection and diffusion) from the gas phase of the target pollutant to the catalyst surface.[44] At high flow rates, the residence time of the gas in the plug flow photocatalytic reactor is too short for the model pollutant gas to be adequately transported to the catalyst surface.

The $\ln(C/C_0)$ versus time plot at different flow rates is shown in Figure S5 (see the Supporting Information file). The maximum kinetic constant (k) for toluene at the lowest flow rate (FR_3) is 0.003 min^{-1}, while the associated correlation coefficient (R^2) is 0.95. For ethylbenzene, the maximum kinetic constant (k) and correlation coefficient (R^2) were 0.0025 min^{-1} and 0.92, respectively. For chlorobenzene, the maximum kinetic constant (k) is 0.0039 min^{-1} and the associated correlation coefficient (R^2) is 0.93.

3.2.4. Effect of Temperature on PCO of VOCs. Adsorption and desorption processes and kinetic reactions may be affected by the temperature of the reactor. The chemical reaction rate constant (k) depends on the activation energy (E_a) and temperature (T) according to the Arrhenius equation. The activation energy is positive ($E_a > 0$) for most reactions, so the reaction rate increases with increasing temperature. The adsorption process is exothermic, and higher temperatures may reduce the adsorption capacity. However, desorption, which is an endothermic process, is favorable at elevated temperatures. There is a balance between these processes, which varies based on specific conditions, and the dominant mechanism affects the overall reaction rate. If desorption is the rate-limiting step, increasing the temperature will increase the reaction rate. Conversely, if adsorption is the limiting factor, decreasing the temperature will lead to the reaction proceeding more rapidly.[45] Therefore, the effect of temperature on the degradation of various pollutants may have been interpreted differently in the literature.[37] The simultaneous adsorption and PCO of toluene, ethylbenzene, and chlorobenzene were monitored for a constant flow rate (FR_2) and constant concentration (CF_2) at four different temperatures between 21 and 35 °C under UVA irradiation. The effect of the reaction temperature on degradation rates of three model pollutants for PU/ZnO NR hybrid samples is shown in Figure 8. As temperature increases, the internal energy and atomic vibrations of pollutant molecules rise, intensifying their irregular motions. By heating the plug flow reactor system, degradation rates for all three pollutants improved as temperatures increased up to 30 °C. However, VOC removal efficiencies decreased when the temperature reached 35 °C. This behavior was attributed to Henry's law, which states that the solubility of gases generally decreases with increasing temperature.[37,46] The maximum removal efficiencies for all three model pollutants were reached at 30 °C and these values were found to be 79%, 66%, and 85% for toluene, ethylbenzene, and chlorobenzene, respectively. The kinetic constants and correlation coefficients related to the removal efficiencies were also calculated and are shown in Figure S6 (see the Supporting Information file). The maximum kinetic constants (k) of toluene, ethylbenzene, and chlorobenzene were calculated as 0.0035, 0.0028, and 0.0048 min^{-1} for the reaction at 30 °C, respectively. Faghihi-Zarandi et al. found that the adsorption capacity and removal efficiency of toluene improved in the range of 0−20 °C, however, partially decreased with increasing temperature in the range of 20−60 °C.[47] Davarpanah et al. reported that during competitive adsorption using beaded activated carbon, the removal efficiency of 1,2,4-trimethylbenzene increased from 85.3% to 92.2% with increasing temperature (20−27 °C) under high humidity conditions.[48] Zorn et al. observed that raising the reaction temperature from 30 to 77 °C increased the reaction rate constant of vapor acetone, but further increasing it to 113 °C had no significant effect.[48]

3.2.5. Effect of RH on PCO of VOCs. In the photocatalytic removal of gaseous organic compounds, the presence of water vapor is one of the main factors affecting the PCO performance (solid−gas interaction). Water molecules are the main source of hydroxyl radicals; therefore, it is not possible to facilitate the PCO process without moisture. Insufficient water content reduces the production of hydroxyl radicals on the catalyst surface, leading to a decrease in photocatalytic performance, as oxidation reactions are not triggered.[49] The basic principle of PCO is that pollutant molecules are decomposed into intermediate products by the oxidation process and further

Downloaded from pubs.acs.org/aanmf6/article-pdf/8/14/7290/4068736/an5c00665.pdf by guest on 17 November 2026

https://doi.org/10.1021/acsanm.5c00665
ACS Appl. Nano Mater. 2025, 8, 7290−7303

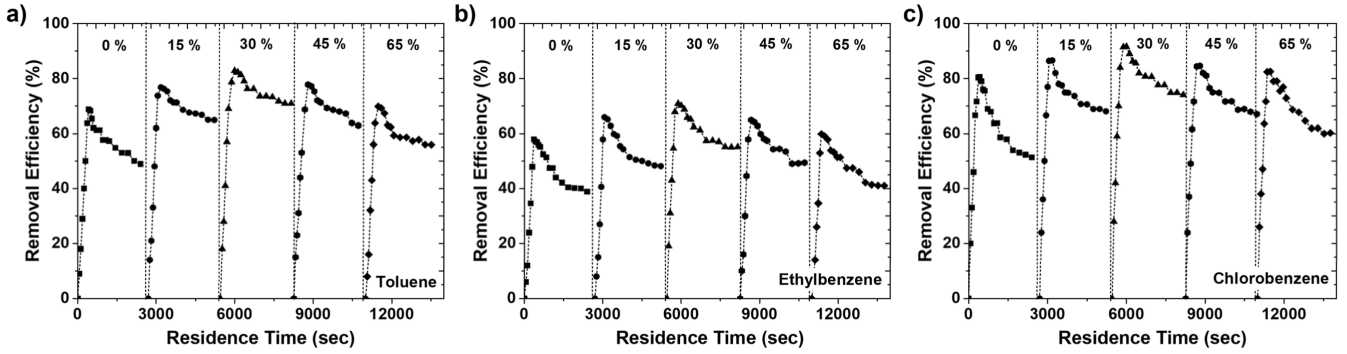

Figure 9. Effect of RH on removal efficiencies of toluene (a), ethylbenzene (b), and chlorobenzene (c) for PU/ZnO NR hybrid samples under UVA light irradiation.

mineralized into harmless inorganic molecules (i.e., H_2O, CO_2, etc.). However, RH has been found to be positively correlated to transformed CO_2, which is directly related to mineralization. The removal efficiencies of toluene, ethylbenzene, and chlorobenzene at different RH (0%, 15%, 30%, 45%, and 65%) for a constant flow rate (FR_2) and constant concentration (C_{F2}) are shown in Figure 9. The degradation rates of pollutants were improved in the presence of RH for three model pollutants. The maximum removal efficiencies were obtained at 30% RH as 81%, 71%, and 92% for toluene, ethylbenzene, and chlorobenzene, respectively. However, a gradual increase in RH from 30% to 65% led to lower reaction rates. The surface of the photocatalyst ZnO NRs is hydrophilic and water molecules tend to adsorb on the surface of the photocatalyst, leading to an inhibition of the adsorption of pollutants onto the photocatalyst and resulted in a decrease in photocatalytic efficiency.[10] The amount of water that can be adsorbed on the ZnO NR surface is greater than that of the monolayer. The overall effect on the adsorption process of active surface sites is probably related to the competition of water molecules with pollutant molecules. Therefore, the hydrophilic effect on the surface dominates the oxidative effect, causing the reaction rates to decrease.[38,50] Photocatalytic reactions occur faster in humid air than in dry air (0% RH), indicating a positive contribution to the reaction kinetics, especially at low humidity levels, such as 15−30% RH. This effect may be interpreted as the contribution of adsorbed water to the renewal of active surface species. H_2O molecules dissociate and adsorb onto the ZnO NR surfaces at low RH and form −OH groups on the surface. The kinetic constants and correlation coefficients associated with the degradation rates were also calculated and are shown in Figure S7 (see the Supporting Information file). The maximum kinetic constants (k) of toluene, ethylbenzene, and chlorobenzene were calculated as 0.0041, 0.0028, and 0.0056 min^{-1} for the reaction at 30% RH, respectively. The correlation coefficients (R^2) associated with them are 0.97, 0.91, and 0.92, respectively. RH is the most effective parameter in PCO processes compared to other parameters (i.e., concentration, flow rate, and temperature), as these values indicate maximum performance.

Sleiman et al. observed that the maximum toluene removal was obtained at 30% RH using a TiO_2 photocatalyst. However, the toluene removal efficiency decreased at 50% and 70% RH.[51] Rismanchian et al. investigated the toluene removal efficiency with TiO_2 nanoparticles coated on nickel metal foam at different humidity levels of 10, 30, 50, and 80%. They found that increasing the humidity level first enhanced the degradation rate of the pollutants, and then increasing the humidity from 30% to 80% decreased the photocatalytic efficiencies.[52] Other studies reported low efficiency at high humidity levels for formaldehyde, acetone,[53] toluene,[54] and NO.[55]

3.2.6. CO_2 Conversion Rate on PCO of VOCs. Toluene, ethylbenzene, and chlorobenzene are decomposed into intermediate products such as benzyl alcohol, benzaldehyde, and benzoic acid by the radicals generated during PCO reactions. $^{\bullet}OH$ and $^{\bullet}O_2^-$ radicals continue to attack the isomerized products, breaking them into short-chain molecules such as acetone, acetaldehyde, acetic acid, and propionic acid.[56,57] Then, these small molecules are completely oxidized to hydrocarbons, CO_2, and H_2O. The most important indicator of PCO is the CO_2 conversion rate, attributed to the mineralization degree of pollutant molecules. The CO_2 concentrations were monitored by the detector at the reactor outlet over time for all of the photocatalytic experiments. The degradation rates, CO_2 conversion rates, kinetic constants, and associated correlation coefficients of toluene, ethylbenzene, and chlorobenzene upon PCO process under different reaction conditions are listed in Table S2 (see the Supporting Information file). The CO_2 conversion rate increased rapidly in the first 8 min and gradually decreased parallel to the pollutant concentration gradients. The CO_2 concentrations were observed in the range 80−100 ppm for toluene, 75−95 ppm for ethylbenzene, and 85−105 ppm for chlorobenzene. Moreover, the time-dependent changes in CO_2 concentrations measured at different temperatures and RH levels for the three model pollutants are shown in Figure S8 (see the Supporting Information file). The detected CO_2 concentration for toluene was 85 ppm at room temperature and increased to 110 ppm with rising temperatures up to 30 °C. The CO_2 concentration decreased slightly as the temperature increased to 35 °C. In dry air conditions (0% RH), the CO_2 concentration for toluene was measured at 85 ppm but increased to 125 ppm when the RH reached 30%. For RH levels exceeding 30%, the concentration dropped to 100 ppm. Even at high humidity levels (>35% RH), CO_2 conversion remained higher compared to dry air. For ethylbenzene and chlorobenzene, the effects of the temperature and RH on the CO_2 conversion rate were parallel to their removal efficiencies. The maximum CO_2 concentrations for ethylbenzene and chlorobenzene were measured as 105 and 125 ppm at 30 °C, respectively. Similarly, with an increase in RH up to 30%, maximum CO_2 concentrations for ethylbenzene and chlorobenzene were determined as 120 and 145 ppm, respectively. There is a partial decrease in the CO_2 conversion rates at higher temperatures and higher humidity levels. Chlorobenzene provided the highest CO_2 conversion rate by

Downloaded from pubs.acs.org/aanmf6/article-pdf/8/14/7290/4068736/an5c00665.pdf by guest on 17 November 2026

https://doi.org/10.1021/acsanm.5c00665
ACS Appl. Nano Mater. 2025, 8, 7290−7303

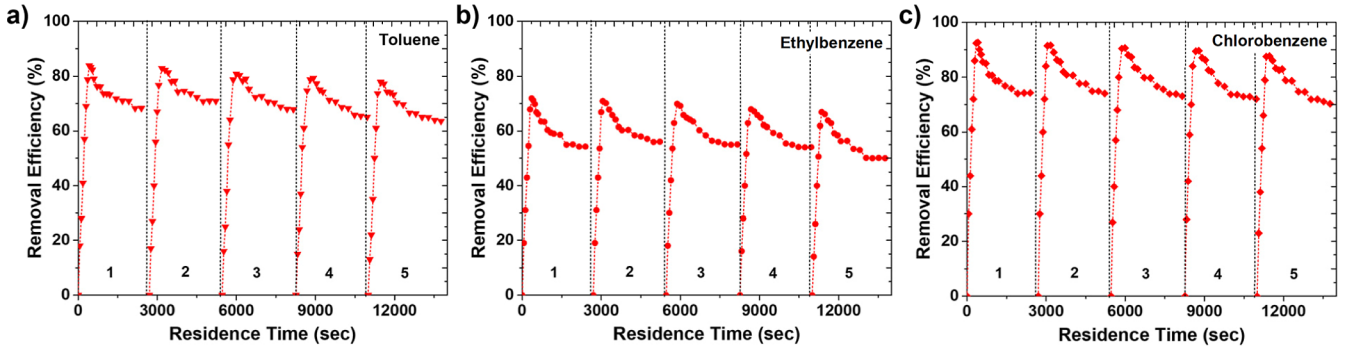

Figure 10. Removal efficiencies of toluene (a), ethylbenzene (b), and chlorobenzene at a constant flow rate (FR_2) and constant concentration (C_{F2}) (c) over five consecutive runs for PU/ZnO NR hybrid samples under UVA light irradiations.

the PU/ZnO NR hybrid structure, which was consistent with the degradation rates. The mineralization efficiencies for the experimental sets exhibiting the highest degradation rates were calculated and are listed in Table S3 (see the Supporting Information file). However, the relatively low CO_2 conversion rates were attributed to the decomposition of pollutant molecules into byproducts and incomplete mineralization. This suggests that the partial oxidation of VOCs leads to the accumulation of oxidized intermediates, which must be considered in assessing the overall photocatalytic efficiency and mineralization extent.

XRD and FT-IR analyses were performed to assess the structural stability of the PU foam under UV irradiation during VOC PCO. The FT-IR spectra and XRD patterns of the samples before and after the experiment are shown in Figure S9 (see the Supporting Information file). The XRD patterns exhibited no detectable change postreaction, confirming the preservation of the structural integrity of the PU foam. The FT-IR spectra showed negligible variations in the absorption bands, indicating no significant chemical transformation of the PU foam. Moreover, no detectable CO_2 evolution was observed following the control experiments conducted to assess the structural stability of the PU foam under UV irradiation. The combined results indicate that the PU foam remains structurally and chemically stable under both UV exposure and VOC contact and that the detected CO_2 originates directly from photocatalytic degradation of the VOCs.

The different removal efficiencies of toluene, ethylbenzene, and chlorobenzene by the PU/ZnO NR hybrid structures were attributed to the physicochemical properties of the pollutants and their interactions with hydrophilic ZnO NRs. Zn^{2+} and O^{2-} ions preferentially adsorb onto polar planes [i.e., (001)] to reduce surface energy during the growth of ZnO NRs.[58] Our previous research revealed that ZnO NRs were Zn^{2+}-terminated and positively charged.[59] Chlorobenzene interacted strongly with the positively charged ZnO surface due to its polar C−Cl bond, leading to effective adsorption. Furthermore, ZnO NRs have a specific surface chemistry that tends to activate chlorinated compounds. The interaction between chlorobenzene and the hydroxyl groups or defect sites of ZnO NRs promotes its degradation more efficiently than does toluene or ethylbenzene. Although chlorobenzene has a lower vapor pressure, its strong surface adsorption overcomes this limitation. On the other hand, toluene, with its higher vapor pressure, more readily occupies the reaction environment, and its nonpolar structure leads to weaker adsorption on the ZnO surface. Steric hindrance of the larger ethyl group contained in ethylbenzene led to a decrease in the adsorption capacity, thus exhibiting the lowest removal efficiency. Moreover, the degradation byproducts of ethylbenzene, such as acetophenone, which is more stable and less reactive, hinder the process.[60] Other studies have reported different trends in the removal efficiencies of these VOCs. Toluene has been found to exhibit a higher degradation efficiency than ethylbenzene, owing to its greater reactivity and simpler degradation pathway under identical conditions. The degradation of chlorobenzene typically generates chlorinated intermediates, such as chlorophenols, which are more toxic and exhibit increased resistance to oxidation.[61,62] These intermediates may act as inhibitors in the photocatalytic process, thereby reducing the removal efficiency. However, studies agree that the less polar toluene and ethylbenzene molecules are inefficiently adsorbed compared to chlorobenzene.[63,64] The possible degradation pathways of toluene, ethylbenzene, and chlorobenzene, as reported in the literature, are schematically illustrated in Figure S10 (see the Supporting Information file). In this study, ZnO NRs have specific surface chemistry that can preferentially activate chlorinated compounds. The interaction of chlorobenzene with the hydroxyl groups or defect sites of ZnO is more efficient compared with toluene or ethylbenzene, emphasizing the significant role of photocatalyst properties, such as the hydrophilicity and surface charge of ZnO NRs, in the degradation of VOCs.

3.2.7. Catalyst Stability Test. Five consecutive photocatalytic experiments were carried out at constant concentration (C_{F2}), constant flow rate (FR_2), and 30% RH to evaluate the stability of the PU/ZnO NR hybrid catalysts. The photocatalyst samples were cleaned after each set of experiments. First, synthetic air was allowed to flow into the reactor at 30% RH for 60 min when the VOC concentration was zero. During this step, the UVA lamp was kept on, promoting the removal of the adsorbed reaction byproducts. Although this cleaning cycle is relatively short and practical for large-scale applications, traces of adsorbed byproducts may remain on the catalyst surface, especially after exposure high concentrations and subsequent deactivation. Therefore, deep cleaning cycles were performed by keeping the samples in the oven at 70 °C for 2 h for activation. The concentration changes of toluene, ethylbenzene, and chlorobenzene over five consecutive runs are shown in Figure S11 (see the Supporting Information file), and the degradation cycles are shown in Figure 10. A negligible decrease in concentration was observed up to the fifth cycle for all three VOCs. Similarly, the degradation rates remained stable. Therefore, the ZnO/PU NR hybrid catalyst may be reused for at least five cycles without any loss of catalytic activity.

Downloaded from pubs.acs.org/aanmf6/article-pdf/8/14/7290/4068736/an5c00665.pdf by guest on 17 November 2026

https://doi.org/10.1021/acsanm.5c00665
ACS Appl. Nano Mater. 2025, 8, 7290−7303

The literature on VOC removal using ZnO-based photocatalysts is relatively limited. A comparative table summarizing selected studies is listed in Table S4 (see the Supporting Information file). The referenced studies used ZnO nanostructures immobilized on various substrates such as activated carbon, zeolites, and perlite granules, and each structure presents different surface areas. Moreover, the reactor types, reaction conditions, and light sources vary significantly.[65−70] Still, the reaction kinetics and removal efficiencies observed in this study are consistent with those reported in related studies.

4. CONCLUSIONS

A flexible hybrid catalyst by ZnO NRs immobilized on a 3D PU foam surface was successfully developed and utilized for VOCs removal for the first time. The functionalization of the PU substrate by chemical treatment provided an optimum surface for strong adhesion of the catalyst. Characterizations such as FTIR, XRD, and SEM confirmed the successful integration of ZnO NRs onto the surface, which is crucial for the stability and performance of the catalyst. The catalyst exhibited an improved performance at relatively high temperatures (i.e., up to 30 °C). Moreover, water vapor significantly influenced the reaction kinetics and increased the degradation rates for all three pollutants. The maximum VOCs removal efficiencies of 81%, 71%, and 92% were obtained for toluene, ethylbenzene, and chlorobenzene, respectively, at 30 °C and 30% RH. The effects of initial concentration and air flow rate were largely dependent on the reactor geometry, and further research is needed to optimize these parameters to improve VOC removal. Despite its complex degradation pathways, chlorobenzene showed a higher removal efficiency than toluene and ethylbenzene. The hydrophilic nature of the ZnO NR surface contributed to the activation of chlorinated compounds, supporting their efficient degradation. The interactions between the pollutants and the hydrophilic surface of the ZnO NRs emphasized the importance of surface chemistry on the photocatalytic activity. The PU/ZnO NR hybrid catalyst maintained its high activity without significant efficiency loss in five consecutive experiments, offering the advantage of reusability for practical applications. The present study highlighted the critical role of catalyst surface properties, environmental conditions, and pollutant characteristics in optimizing the photocatalytic removal of VOCs. New research efforts focus on enhancing catalyst resistance to deactivation and understanding byproduct formation to further improve photocatalytic efficiency and sustainability.

■ ASSOCIATED CONTENT

Supporting Information

The Supporting Information is available free of charge at https://pubs.acs.org/doi/10.1021/acsanm.5c00665.

Schematic illustration of PFR; EDS spectra; VOC concentration changes for the control and photolysis tests; the first-order kinetic curves; the CO_2 concentration changes; VOC concentration changes for catalyst stability tests; summary of photocatalytic efficiencies, kinetics, and CO_2 production; XRD patterns and FT-IR spectra; degradation pathways; and comparison of related studies (PDF)

■ AUTHOR INFORMATION

Corresponding Author

Memnune Kardeş − *Department of Materials Science and Engineering, Gebze Technical University, Gebze, Kocaeli 41400, Turkey; Faculty of Engineering and Natural Sciences, Integrated Manufacturing Technologies Center of Excellence, Sabanci University, Istanbul 34956, Turkey;* orcid.org/0000-0002-5073-6564; Email: memnunedaglar@gtu.edu.tr

Authors

Bekir Dizman − *Faculty of Engineering and Natural Sciences, Integrated Manufacturing Technologies Center of Excellence, Sabanci University, Istanbul 34956, Turkey;* orcid.org/0000-0002-4909-8403

Koray Öztürk − *Department of Materials Science and Engineering, Gebze Technical University, Gebze, Kocaeli 41400, Turkey;* orcid.org/0000-0003-1795-0777

Derya Y. Köseoğlu-İmer − *Department of Environmental Engineering, Istanbul Technical University, Istanbul 34396, Turkey;* orcid.org/0000-0003-3023-4556

Complete contact information is available at: https://pubs.acs.org/10.1021/acsanm.5c00665

Author Contributions

‖B.D., K.Ö., D.Y. K.-İ. contributed equally to this paper. M. K. contributed to the conception and design of the study, project administration, term development, visualization, data curation, investigation, formal analysis, methodology, validation, and the preparation of the original draft. B. D., K. Ö., and D.Y. K.-İ. contributed equally to the supervision, term development, conceptualization, formal analysis, validation, and writing of the manuscript. All authors have given approval to the final version of the manuscript.

Funding

This study was funded by the Scientific and Technical Research Council of Turkey (TUBITAK) within the scope of the project no. 121C471.

Notes

The authors declare no competing financial interest.

■ ACKNOWLEDGMENTS

M. K. gratefully acknowledges the financial support provided by TUBITAK within the scope of project number 121C471 of the 2218-Postdoctoral Researcher Program. The authors are grateful to TUBITAK for their financial support and Sabanci University Integrated Manufacturing Technologies Center of Excellence Laboratory where the photocatalytic experiments were performed.

■ REFERENCES

(1) Tang, X.; Misztal, P. K.; Nazaroff, W. W.; Goldstein, A. H. Volatile Organic Compound Emissions from Humans Indoors. *Environ. Sci. Technol.* **2016**, *50* (23), 12686−12694.

(2) Wang, N.; Ernle, L.; Bekö, G.; Wargocki, P.; Williams, J. Emission Rates of Volatile Organic Compounds from Humans. *Environ. Sci. Technol.* **2022**, *56* (8), 4838−4848.

(3) He, C.; Cheng, J.; Zhang, X.; Douthwaite, M.; Pattisson, S.; Hao, Z. Recent Advances in the Catalytic Oxidation of Volatile Organic Compounds: A Review Based on Pollutant Sorts and Sources. *Chem. Rev.* **2019**, *119* (7), 4471−4568.

(4) Mamaghani, A. H.; Haghighat, F.; Lee, C. S. Photocatalytic Oxidation Technology for Indoor Environment Air Purification: The State-of-the-Art. *Appl. Catal., B* **2017**, *203*, 247−269.

Downloaded from pubs.acs.org/aanmf6/article-pdf/8/14/7290/4068736/an5c00665.pdf by guest on 17 November 2026

(5) Li, X.; Zhang, L.; Yang, Z.; Wang, P.; Yan, Y.; Ran, J. Adsorption Materials for Volatile Organic Compounds (VOCs) and the Key Factors for VOCs Adsorption Process: A Review. *Sep. Purif. Technol.* **2020**, *235*, 116213.
(6) Kamal, M. S.; Razzak, S. A.; Hossain, M. M. Catalytic Oxidation of Volatile Organic Compounds (VOCs) − A Review. *Atmos. Environ.* **2016**, *140*, 117−134.
(7) Yang, C.; Miao, G.; Pi, Y.; Xia, Q.; Wu, J.; Li, Z.; Xiao, J. Abatement of Various Types of VOCs by Adsorption/Catalytic Oxidation: A Review. *Chem. Eng. J.* **2019**, *370*, 1128−1153.
(8) Shah, K. W.; Li, W. A Review on Catalytic Nanomaterials for Volatile Organic Compounds VOC Removal and Their Applications for Healthy Buildings. *Nanomaterials* **2019**, *9* (6), 910.
(9) Xie, W.; Li, Y.; Shi, W.; Zhao, L.; Zhao, X.; Fang, P.; Zheng, F.; Wang, S. Novel Effect of Significant Enhancement of Gas-Phase Photocatalytic Efficiency for Nano ZnO. *Chem. Eng. J.* **2012**, *213*, 218−224.
(10) Jafari, A. J.; Kalantari, R. R.; Kermani, M.; Firooz, M. H. Photocatalytic Oxidation of Benzene by ZnO Coated on Glass Plates under Simulated Sunlight. *Chem. Pap.* **2019**, *73* (3), 635−644.
(11) Sun, W.; Meng, S.; Zhang, S.; Zheng, X.; Ye, X.; Fu, X.; Chen, S. Insight into the Transfer Mechanisms of Photogenerated Carriers for Heterojunction Photocatalysts with the Analogous Positions of Valence Band and Conduction Band: A Case Study of ZnO/TiO_2. *J. Phys. Chem. C* **2018**, *122* (27), 15409−15420.
(12) Le Pivert, M.; Kerivel, O.; Zerelli, B.; Leprince-Wang, Y. ZnO Nanostructures Based Innovative Photocatalytic Road for Air Purification. *J. Cleaner Prod.* **2021**, *318*, 128447.
(13) Razote, B. J.; Tayyab, M.; Shin, D.; Kim, K. M.; Lee, C. H. Enhancing Photothermal VOCs Removal in ZnO-Based Catalysts via Transition Metal-Based Band Edge Tuning and Oxygen Vacancy Engineering. *J. Environ. Chem. Eng.* **2023**, *11* (2), 109565.
(14) Samadi, M.; Zirak, M.; Naseri, A.; Kheirabadi, M.; Ebrahimi, M.; Moshfegh, A. Z. Design and Tailoring of One-Dimensional ZnO Nanomaterials for Photocatalytic Degradation of Organic Dyes: A Review. *Res. Chem. Intermed.* **2019**, *45* (4), 2197−2254.
(15) Le, A. T.; Le, T. D. H.; Cheong, K. Y.; Pung, S. Y. Immobilization of Zinc Oxide-Based Photocatalysts for Organic Pollutant Degradation: A Review. *J. Environ. Chem. Eng.* **2022**, *10* (5), 108505.
(16) De Mimérand, Y. D. R.; Li, K.; Zhou, C.; Jin, X.; Hu, X.; Chen, Y.; Guo, J. Functional Supported ZnO/Bi_2MoO_6 Heterojunction Photocatalysts with 3D-Printed Fractal Polymer Substrates and Produced by Innovative Plasma-Based Immobilization Methods. *ACS Appl. Mater. Interfaces* **2020**, *12* (38), 43138−43151.
(17) Feng, S.; Li, D.; Low, Z. x.; Liu, Z.; Zhong, Z.; Hu, Y.; Wang, Y.; Xing, W. ALD-Seeded Hydrothermally-Grown Ag/ZnO Nanorod PTFE Membrane as Efficient Indoor Air Filter. *J. Membr. Sci.* **2017**, *531*, 86−93.
(18) Chae, S.; Yu, J.; Oh, J. Y.; Lee, T. I. Hybrid Poly (3-Hexylthiophene) (P3HT) Nanomesh/ZnO Nanorod p-n Junction Visible Photocatalyst for Efficient Indoor Air Purification. *Appl. Surf. Sci.* **2019**, *496*, 143641.
(19) Noorisafa, F.; Razmjou, A.; Emami, N.; Low, Z. X.; Korayem, A. H.; Kajani, A. A. Surface Modification of Polyurethane via Creating a Biocompatible Superhydrophilic Nanostructured Layer: Role of Surface Chemistry and Structure. *J. Exp. Nanosci.* **2016**, *11* (14), 1087−1109.
(20) Chandan, M. R.; Radhakrishnan, K.; Bal, D. K.; Rizwan, M.; Shaik, A. H. Flexible Polyurethane Foam-ZnO Nanocomposite for Photocatalytic Degradation of Textile Dye. *Fibers Polym.* **2020**, *21* (10), 2314−2320.
(21) Pham, T. D.; Lee, B. K. Novel Adsorption and Photocatalytic Oxidation for Removal of Gaseous Toluene by V-Doped TiO_2/PU under Visible Light. *J. Hazard. Mater.* **2015**, *300*, 493−503.
(22) Freitas, C.; Severino, M. I.; Mohtar, A. A.; Kolmykov, O.; Pimenta, V.; Nouar, F.; Serre, C.; Pinto, M. Metal-Organic Frameworks Polyurethane Composite Foams for the Capture of Volatile Organic Compounds. *ACS Mater. Lett.* **2024**, *6* (1), 174−181.
(23) He, Z.; Zhou, L.; Li, G.; Zeng, X.; An, T.; Sheng, G.; Fu, J.; Bai, Z. Comparative Study of the Eliminating of Waste Gas Containing Toluene in Twin Biotrickling Filters Packed with Molecular Sieve and Polyurethane Foam. *J. Hazard. Mater.* **2009**, *167* (1−3), 275−281.
(24) Huang, H.; Xie, X.; Xiao, F.; Liu, B.; Zhang, T.; Feng, F.; Lan, B.; Zhang, C. A Critical Review of Deep Oxidation of Gaseous Volatile Organic Compounds via Aqueous Advanced Oxidation Processes. *Environ. Sci. Technol.* **2024**, *58* (42), 18456−18473.
(25) Grall, A. J.; Zellers, E. T.; Sacks, R. D. High-Speed Analysis of Complex Indoor VOC Mixtures by Vacuum-Outlet GC with Air Carrier Gas and Programmable Retention. *Environ. Sci. Technol.* **2001**, *35* (1), 163−169.
(26) Kardeş, M.; Yatmaz, H. C.; Öztürk, K. ZnO Nanorods Grown on Flexible Polyurethane Foam Surfaces for Photocatalytic Azo Dye Treatment. *ACS Appl. Nano Mater.* **2023**, *6* (8), 6605−6613.
(27) Kardeş, M.; Başaran Dindaş, G.; Yatmaz, H. C.; Dizge, N.; Öztürk, K. CBD Grown Pure and Ce-Doped ZnO Nanorods: Comparison of Their Photocatalytic Degrading Efficiencies on AR88 Azo Dye under Visible Light Irradiation. *Colloids Surf., A* **2020**, *607*, 125451.
(28) Ponnamma, D.; Cabibihan, J. J.; Rajan, M.; Pethaiah, S. S.; Deshmukh, K.; Gogoi, J. P.; Pasha, S. K. K.; Ahamed, M. B.; Krishnegowda, J.; Chandrashekar, B. N.; Polu, A. R.; Cheng, C. Synthesis, Optimization and Applications of ZnO/Polymer Nanocomposites. *Mater. Sci. Eng., C* **2019**, *98*, 1210−1240.
(29) Trovati, G.; Sanches, E. A.; Neto, S. C.; Mascarenhas, Y. P.; Chierice, G. O. Characterization of Polyurethane Resins by FTIR, TGA, and XRD. *J. Appl. Polym. Sci.* **2010**, *115* (1), 263−268.
(30) Alves, P.; Coelho, J. F. J.; Haack, J.; Rota, A.; Bruinink, A.; Gil, M. H. Surface Modification and Characterization of Thermoplastic Polyurethane. *Eur. Polym. J.* **2009**, *45* (5), 1412−1419.
(31) Cui, C. W.; Yang, C.; Bao, J.; Huang, X. J.; Zeng, X. F.; Chen, J. F. Monodispersed ZnO Nanoparticle-Poly(Methyl Methacrylate) Composites with Visible Transparency for Ultraviolet Shielding Applications. *ACS Appl. Nano Mater.* **2020**, *3* (9), 9026−9034.
(32) Hussein, M. A.; Alamry, K. A.; Almehmadi, S. J.; Elfaky, M. A.; Džudžević-Čančar, H.; Asiri, A. M.; Hussien, M. A. Novel Biologically Active Polyurea Derivatives and Its TiO_2-Doped Nanocomposites. *Des. Monomers Polym.* **2020**, *23* (1), 59−74.
(33) Kumar, V.; Gupta, R.; Bansal, A. Hydrothermal Growth of ZnO Nanorods for Use in Dye-Sensitized Solar Cells. *ACS Appl. Nano Mater.* **2021**, *4* (6), 6212−6222.
(34) Qiu, J.; Guo, M.; Wang, X. Electrodeposition of Hierarchical ZnO Nanorod-Nanosheet Structures and Their Applications in Dye-Sensitized Solar Cells. *ACS Appl. Mater. Interfaces* **2011**, *3* (7), 2358−2367.
(35) Inayat, A.; Freund, H.; Zeiser, T.; Schwieger, W. Determining the Specific Surface Area of Ceramic Foams: The Tetrakaidecahedra Model Revisited. *Chem. Eng. Sci.* **2011**, *66* (6), 1179−1188.
(36) Belkessa, N.; Serhane, Y.; Bouzaza, A.; Khezami, L.; Assadi, A. A. Gaseous Ethylbenzene Removal by Photocatalytic TiO_2 Nanoparticles Immobilized on Glass Fiber Tissue under Real Conditions: Evaluation of Reactive Oxygen Species Contribution to the Photocatalytic Process. *Environ. Sci. Pollut. Res.* **2023**, *30* (13), 35745−35756.
(37) Yan, X.; Anguille, S.; Bendahan, M.; Moulin, P. Toluene Removal from Gas Streams by an Ionic Liquid Membrane: Experiment and Modeling. *Chem. Eng. J.* **2021**, *404*, 127109.
(38) Quici, N.; Vera, M. L.; Choi, H.; Puma, G. L.; Dionysiou, D. D.; Litter, M. I.; Destaillats, H. Effect of Key Parameters on the Photocatalytic Oxidation of Toluene at Low Concentrations in Air under 254 + 185 Nm UV Irradiation. *Appl. Catal., B* **2010**, *95* (3−4), 312−319.
(39) Mamaghani, A. H.; Haghighat, F.; Lee, C. S. Photocatalytic Oxidation Technology for Indoor Environment Air Purification: The State-of-the-Art. *Appl. Catal., B* **2017**, *203*, 247−269.
(40) Ma, J.; Zhu, C.; Lu, J.; Liu, H.; Huang, L.; Chen, T.; Chen, D. Catalytic Degradation of Gaseous Benzene by Using TiO_2/Goethite Immobilized on Palygorskite: Preparation, Characterization and Mechanism. *Solid State Sci.* **2015**, *49*, 1−9.

Downloaded from pubs.acs.org/aanmf6/article-pdf/8/14/7290/4068736/an5c00665.pdf by guest on 17 November 2026

(41) Rezaee, A.; Rangkooy, H.; Khavanin, A.; Jafari, A. J. High Photocatalytic Decomposition of the Air Pollutant Formaldehyde Using Nano-ZnO on Bone Char. *Environ. Chem. Lett.* **2014**, *12* (2), 353−357.
(42) Chen, R.; Zhu, C.; Lu, J.; Xiao, J.; Lei, Y.; Yu, Z. $BiVO_4/\alpha$-Fe_2O_3 Catalytic Degradation of Gaseous Benzene: Preparation, Characterization and Photocatalytic Properties. *Appl. Surf. Sci.* **2018**, *427*, 141−147.
(43) Malayeri, M.; Lee, C. S.; Haghighat, F.; Klimes, L. Modeling of Gas-Phase Heterogeneous Photocatalytic Oxidation Reactor in the Presence of Mass Transfer Limitation and Axial Dispersion. *Chem. Eng. J.* **2020**, *386* (October 2019), 124013.
(44) Jo, W. K.; Kim, J. T. Application of Visible-Light Photocatalysis with Nitrogen-Doped or Unmodified Titanium Dioxide for Control of Indoor-Level Volatile Organic Compounds. *J. Hazard. Mater.* **2009**, *164* (1), 360−366.
(45) Vuong, M. D.; Couvert, A.; Couriol, C.; Amrane, A.; Le Cloirec, P.; Renner, C. Determination of the Henry's Constant and the Mass Transfer Rate of VOCs in Solvents. *Chem. Eng. J.* **2009**, *150* (2), 426−430.
(46) Davarpanah, M.; Rahmani, K.; Kamravaei, S.; Hashisho, Z.; Crompton, D.; Anderson, J. E. Modeling the Effect of Humidity and Temperature on VOC Removal Efficiency in a Multistage Fluidized Bed Adsorber. *Chem. Eng. J.* **2022**, *431*, 133991.
(47) Faghihi-Zarandi, A.; Shirkhanloo, H.; Jamshidzadeh, C. A New Method for Removal of Hazardous Toluene Vapor from Air Based on Ionic Liquid-Phase Adsorbent. *Int. J. Environ. Sci. Technol.* **2019**, *16* (6), 2797−2808.
(48) Zorn, M. E.; Tompkins, D. T.; Zeltner, W. A.; Anderson, M. A. Photocatalytic Oxidation of Acetone Vapor on TiO_2/ZrO_2 Thin Films. *Appl. Catal., B* **1999**, *23* (1), 1−8.
(49) Tomašić, V.; Jović, F.; Gomzi, Z. Photocatalytic Oxidation of Toluene in the Gas Phase: Modelling an Annular Photocatalytic Reactor. *Catal. Today* **2008**, *137* (2−4), 350−356.
(50) Ketteler, G.; Yamamoto, S.; Bluhm, H.; Andersson, K.; Starr, D. E.; Ogletree, D. F.; Ogasawara, H.; Nilsson, A.; Salmeron, M. The Nature of Water Nucleation Sites on TiO_2(110) Surfaces Revealed by Ambient Pressure X-Ray Photoelectron Spectroscopy. *J. Phys. Chem. C* **2007**, *111* (23), 8278−8282.
(51) Sleiman, M.; Conchon, P.; Ferronato, C.; Chovelon, J. M. Photocatalytic Oxidation of Toluene at Indoor Air Levels (Ppbv): Towards a Better Assessment of Conversion, Reaction Intermediates and Mineralization. *Appl. Catal., B* **2009**, *86* (3−4), 159−165.
(52) Rismanchian, M.; Akbari, J.; Keshavarzi, R. Photocatalytic Removal of Gaseous Toluene by Titanium Dioxide Coated on Nickel Foam: Influence of Relative Humidity and Toluene Concentration. *Int. J. Environ. Health Eng.* **2014**, *3* (1), 29.
(53) Kim, S. B.; Hong, S. C. Kinetic Study for Photocatalytic Degradation of Volatile Organic Compounds in Air Using Thin Film TiO_2 Photocatalyst. *Appl. Catal., B* **2002**, *35* (4), 305−315.
(54) Cao, L.; Gao, Z.; Suib, S.; Obee, T.; Hay, S. O.; Freihaut, J. D. Photocatalytic Oxidation of Toluene on Nanoscale TiO_2 Catalysts: Studies of Deactivation and Regeneration. *J. Catal.* **2000**, *196* (2), 253−261.
(55) Ao, C. H.; Lee, S. C. Indoor Air Purification by Photocatalyst TiO_2 Immobilized on an Activated Carbon Filter Installed in an Air Cleaner. *Chem. Eng. Sci.* **2005**, *60* (1), 103−109.
(56) Buyukada-Kesici, E.; Kardeş, M.; Erturaç Karagöz, K.; Başaran-Dindaş, G.; Öztürk, K.; Cengiz Yatmaz, H.; Koseoglu-Imer, D. Y. Developing of Reticulated Ceramic Photocatalyst for Efficient Photocatalytic Oxidation of Gaseous Toluene. *Chem. Eng. J.* **2023**, *455*, 140672.
(57) Cheng, Z. W.; Feng, L.; Chen, J. M.; Yu, J. M.; Jiang, Y. F. Photocatalytic Conversion of Gaseous Ethylbenzene on Lanthanum-Doped Titanium Dioxide Nanotubes. *J. Hazard. Mater.* **2013**, *254*−*255* (1), 354−363.
(58) Gao, P. X.; Wang, Z. L. Substrate Atomic-Termination-Induced Anisotropie Growth of ZnO Nanowires/Nanorods by the VLS Process. *J. Phys. Chem. B* **2004**, *108* (23), 7534−7537.
(59) Kardeş, M.; Öztürk, K. A Comparative Investigation of Photocatalyst ZnO Nanorods Grown on Different Seed Layers: Influence of Annealing Temperature and Atmosphere. *Res. Chem. Intermed.* **2024**, *50* (1), 353−372.
(60) Azeez, M. O.; Nafiu, S. A.; Olarewaju, T. A.; Olabintan, A. B.; Tanimu, A.; Gambo, Y.; Aitani, A. Selective Catalytic Oxidation of Ethylbenzene to Acetophenone: A Review of Catalyst Systems and Reaction Mechanisms. *Ind. Eng. Chem. Res.* **2023**, *62* (33), 12795−12828.
(61) Shi, Y.; Zhang, C.; Yang, Z.; Liu, X.; Zhang, X.; Ling, C.; Cheng, J.; Liang, C.; Mao, C.; Zhang, L. Interfacial Electrostatic Field Boosted Exciton Dissociation of Phosphorylated BiOBr for Efficient O_2 Activation and Chlorobenzene Degradation. *J. Phys. Chem. C* **2022**, *126* (51), 21847−21856.
(62) Zhang, L.; Sawell, S.; Moralejo, C.; Anderson, W. A. Heterogeneous Photocatalytic Decomposition of Gas-Phase Chlorobenzene. *Appl. Catal., B* **2007**, *71* (3−4), 135−142.
(63) Cheng, Z.; Sun, P.; Lu, L.; Chen, J.; Jiang, L.; Yu, J. The Interaction Mechanism and Characteristic Evaluation of Ethylbenzene/Chlorobenzene Binary Mixtures Treated by Ozone-Assisted UV254nm Photodegradation. *Sep. Purif. Technol.* **2014**, *132*, 62−69.
(64) Qin, L.; Zhao, B.; Chen, W.; Han, Y.; Wan, Y.; Liu, L.; Lu, H.; Han, J. Simultaneous Removal of Toluene and Chlorobenzene in a Nonthermal Plasma-Catalysis Reactor Packed with Fe1-Mn1/γ-Al_2O_3. *J. Cleaner Prod.* **2022**, *363*, 132611.
(65) Shojaei, A.; Ghafourian, H.; Yadegarian, L.; Lari, K.; Sadatipour, M. T. Removal of Volatile Organic Compounds (VOCs) from Waste Air Stream Using Ozone Assisted Zinc Oxide (ZnO) Nanoparticles Coated on Zeolite. *J. Environ. Health Sci. Eng.* **2021**, *19* (1), 771−780.
(66) Kang, S.; Park, D. h.; Hwang, J. Hierarchical ZnO Nano-Spines Grown on a Carbon Fiber Seed Layer for Efficient VOC Removal and Airborne Virus and Bacteria Inactivation. *J. Hazard. Mater.* **2022**, *424*, 127262.
(67) Ranjbari, A.; Demeestere, K.; Walgraeve, C.; Kim, K. H.; Heynderickx, P. M. Novel Kinetic Modeling of Photocatalytic Degradation of Ethanol and Acetaldehyde in Air by Commercial and Reduced ZnO: Effect of Oxygen Vacancies and Humidity. *Chemosphere* **2024**, *358*, 142118.
(68) Zhao, X.; Zhao, W.; Chen, Z.; Liu, C.; Zhou, Y.; Zhu, Z.; Yang, Y.; Qi, J.; Li, J. Hierarchical Porous Carbon Spheres Using Nano-ZnO as a Template to Remove Benzene and Ethyl Acetate. *J. Environ. Chem. Eng.* **2024**, *12* (6), 114799.
(69) Saucedo-Lucero, J. O.; Arriaga, S. Study of ZnO-Photocatalyst Deactivation during Continuous Degradation of n-Hexane Vapors. *J. Photochem. Photobiol., A* **2015**, *312*, 28−33.
(70) Jafari, A. J.; Arfaeinia, H.; Badi, M. Y.; Kalantary, R. R.; Kermani, M. Ozone-Assisted Photocatalytic Degradation of Benzene Using Nano-Zinc Oxide Impregnated Granular Activated Carbon (ZnO−GAC) in a Continuous Fluidized Bed Reactor. *Environ. Prog. Sustain. Energy* **2019**, *38* (4), 13082.

Downloaded from pubs.acs.org/aanmf6/article-pdf/8/14/7290/4068736/an5c00665.pdf by guest on 17 November 2026

https://doi.org/10.1021/acsanm.5c00665
ACS Appl. Nano Mater. 2025, 8, 7290−7303